Infrared Physics & Technology 54 (2011) 233–236

Contents lists available at ScienceDirect

Infrared Physics & Technology

journal homepage: www.elsevier.com/locate/infrared

# Spectral response and device performance tuning of long-wavelength InAs QDIPs

H.S. Ling [a,*], S.Y. Wang [a], C.P. Lee [b]

[a] Institute of Astronomy and Astrophysics, Academia Sinica, PO. Box 23-141, Taipei, Taiwan
[b] Department of Electronic Engineering, National Chiao Tung University, 1001 Ta Hsueh Road, Hsinchu 300, Taiwan

ARTICLE INFO

*Article history:*
Available online 25 December 2010

*Keywords:*
Quantum dot
Intersubband
Infrared detector

ABSTRACT

Long-wavelength InAs QDIPs with different thicknesses of InGaAs cap layer in the confinement-enhanced dots-in-a-well (CE-DWELL) structure were investigated. The sample with 3 nm cap layer shows primarily single band detection at 7 μm that stems from the transition between QD states, but the 5 nm and 7 nm samples reveal voltage-tunable dual band detection in the region of 6–11 μm from transitions to the states in the dots as well as the states in the well. The wavefunction coupling of transition states is effectively modified by the change of cap-layer thickness and the bias polarity, which leads to the observed spectral change and demonstrates the flexibility of the CE-DWELL QDIPs. For higher peak quantum efficiency (QE), thin InGaAs cap layers are used to obtain focused absorption strength. With 3 nm cap layer in the CE-DWELL, a respectable QE of 7.23% is reached for 10-stack QDIPs with 7 μm detection wavelength at 77 K, and a high detectivity of $3.4 \times 10^{10}$ Jones is also obtained.

© 2010 Elsevier B.V. All rights reserved.

## 1. Introduction

Long-wavelength (8–12 μm) infrared (LWIR) detectors are essential to the thermal radiation detection of room temperature objects. For such applications, quantum-dot infrared photodetectors (QDIPs) have been widely studied in the past decade because of the potential in low cost and high operating temperatures [1–10]. With the self-assembled In(Ga)As/GaAs QDs, several encouraging results have been demonstrated with operation temperatures higher than 200 K [1] and even up to room temperature [2,3]. However, the detection wavelengths of the QDIPs with common QD structures are out of the LWIR atmospheric transmission window and, unfortunately, cannot be easily adjusted to the desired LWIR band due to the limitation of the self-assembled growth process of QDs. In order to fit the detection band into the LWIR window, many efforts have been focused on the QDIPs with dots-in-a-well (DWELL) structures [6–9]. The additional quantum well (QW) in the DWELL structure provides the flexibility in tuning the detection wavelength. Furthermore, to solve the inherently lower quantum efficiency (QE) of the DWELL structure, we have recently developed a confinement-enhanced DWELL (CE-DWELL) design. The CE-DWELL structure utilizes a thin AlGaAs layer on InAs QDs to improve electron wavefunction confinement and thereby enhance the oscillator strength. The QE is greatly enhanced by an order of magnitude [10] and the LWIR QDIPs with operating temperatures over 200 K have been demonstrated [11].

In our previous analysis, the infrared response peak of the CE-DWELL QDIPs originates from the intersubband transition between QD states [10]. The transitions between the QD states and the states in the well, which is commonly observed by other groups [6–9], is not observed in our previous samples and the reason is however not clear. The factor that controls the selection of different intersubband transition paths is essential but has not been reported to date. In this paper, we report the tailoring of spectral response by selecting different intersubband transition paths in QDIPs from different InGaAs cap-layer thickness in the CE-DWELL structures.

## 2. Experiments

Three QDIP samples with different InGaAs cap-layer thicknesses in the CE-DWELL structure were used in this study. They were prepared by a Veeco GEN-II molecular beam epitaxy system on (0 0 1) semi-insulating GaAs substrates. The schematics of the sample structures were shown in Fig. 1. The active region of every sample consists of 10 stacks of CE-DWELL unit (2 nm bottom $In_{0.15}Ga_{0.85}As$/2.2 MLs InAs/2 nm $Al_{0.3}Ga_{0.7}As$/w nm top $In_{0.15}Ga_{0.85}As$) with GaAs barrier layers. A delta-doped Si layer with sheet density of $4 \times 10^{10}$ cm$^{-2}$ was deposited 2 nm below each QD layer. The only factor varied was the thickness of the $In_{0.15}Ga_{0.85}As$ cap layer ($w$ = 3 nm, 5 nm, 7 nm for samples A, B, C respectively). The matrix structure under the QD layer was kept to preserve the optimized QD condition. Uniform QDs with densities about $4 \times 10^{10}$ cm$^{-2}$ were observed in all samples through AFM measurement.

The photoluminescence (PL) and PL excitation (PLE) spectroscopy were used to probe the electronic state energy of each sample

* Corresponding author. Address: Room 620 in Building Engineering 4, 1001 Ta Hsueh Road, Hsinchu 300, Taiwan Tel.: +886 3 5712121x54248.
*E-mail address:* hhling@asiaa.sinica.edu.tw (H.S. Ling).

1350-4495/$ - see front matter © 2010 Elsevier B.V. All rights reserved.
doi:10.1016/j.infrared.2010.12.020

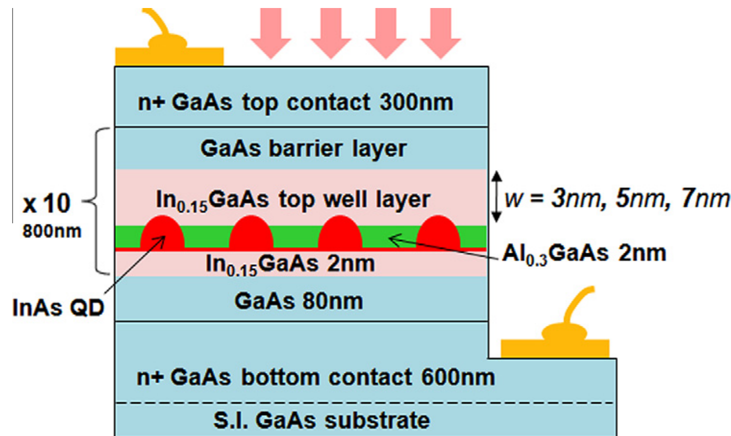


**Fig. 1.** The schematic epitaxy structure of the samples.

at 77 K. The results were shown in Fig. 2. The transition peaks from the lowest 2D QW states were marked by arrows. The transition energy of the 2D state decreases sequentially from samples A to C. The decrease of transition energy agrees with the thickness of the $In_{0.15}Ga_{0.85}As$ cap layer, which is intentionally grown thicker and thicker from samples A to C. Besides, the 2D state peak grows narrower and stronger relative to the GaAs absorption edge in Fig. 2 from samples A to C. The phenomenon suggests that for the three samples the 2D quantum state built up in sample C possesses the most concentrated wavefunction, i.e. the most deeply bound state. The wavefunction coupling of the QD ground state and the 2D state should be better in sample C than in sample B, and than in sample A. On the other hand, the ground state ($\Psi_o$) energy becomes higher with the increase of the total indium content in the CE-DWELL structure. It is attributed to the more pronounced In-Ga intermixing in InAs QDs (grown at 540 °C) due to the stronger In segregation within the thicker InGaAs overlayer that results a Ga-rich region near QDs [12,13].

Standard processing techniques were then applied for the device fabrication. $260 \times 370\ \mu m^2$ mesas with AuGe contact rings were formed to allow normal incidence measurement from the mesa top. In all measurements, the bottom contact is referred as ground. The photocurrent spectra were measured by a Nicholet-550 Fourier transform infrared spectrometer, and the absolute responsivity was calibrated by a 1273 K blackbody radiation source with a Ge wafer to filter out photons with wavelength shorter than 2 μm. Besides, the noise level of the device was obtained with a liquid helium dewar. The noise spectrum was measured by feeding the amplified dark current into a SR-770 fast Fourier transform spectrum analyzer.

## 3. Results and discussion

The normalized photocurrent spectra of the samples at both bias polarities are displayed in Fig. 3. In sample A, a main response peak at 7 μm with a small shoulder peak around 5.5 μm is observed, and the spectra are almost the same at both bias polarities. Combined with the PL and PLE spectroscopy, assuming $\Delta E_{c}:{}_{\Delta E_v}$ = 2: 1, the peak with longer wavelength is attributed to the transition between the QD ground state ($\Psi_o$) and the QD excited state

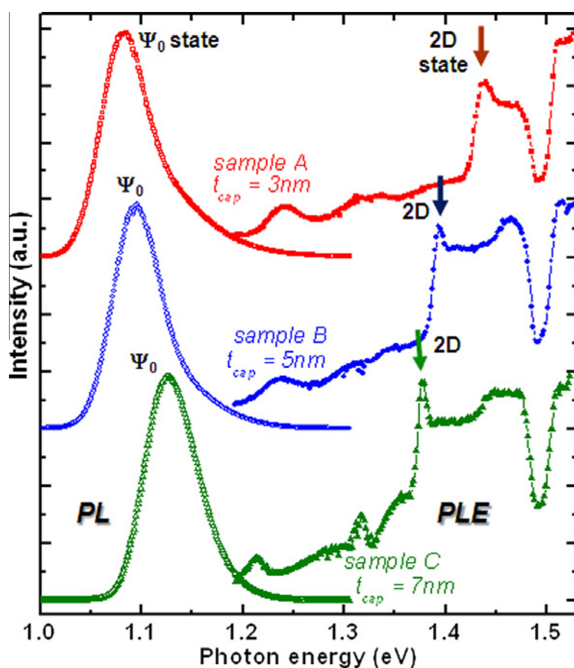


**Fig. 2.** PL and PLE spectra of each sample at 77 K.

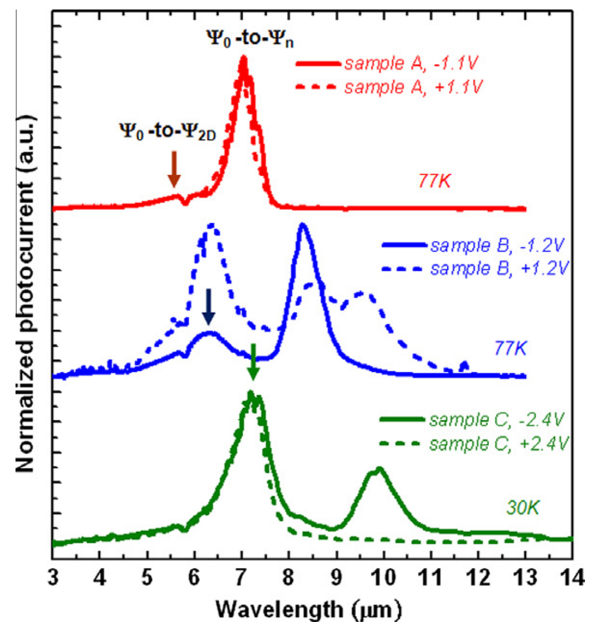


**Fig. 3.** Normalized photocurrent spectra of each sample at positive and negative biases.

($\Psi_n$) while the one with shorter wavelength pertains to the photo-excitation from $\Psi_o$ to the 2D state of the $In_{0.15}Ga_{0.85}As$ QW ($\Psi_{2D}$). Such a dual band detection characteristic is more announced in samples B and C. For sample B, clearer $\Psi_o$-to-$\Psi_{2D}$ transition peak shifts to 6.3 μm and the $\Psi_o$-to-$\Psi_n$ peak shifts to 8.3 μm. Besides, the $\Psi_o$-to-$\Psi_{2D}$ peak becomes stronger than the $\Psi_o$-to-$\Psi_n$ peak when the bias polarity changes from negative to positive. For sample C, the $\Psi_o$-to-$\Psi_{2D}$ peak, which now shifts to 7.2 μm, turns even stronger to dominate the spectrum over the $\Psi_o$-to-$\Psi_n$ peak at 9.9 μm. Furthermore, only the $\Psi_o$-to-$\Psi_{2D}$ peak survives in the spectrum at positive bias.

The response peak due to the $\Psi_o$-to-$\Psi_{2D}$ transition continuously red-shifts, grows, and finally dominates the spectrum over the peak due to the $\Psi_o$-to-$\Psi_n$ transition with thicker and thicker $In_{0.15}Ga_{0.85}As$ cap layer in the CE-DWELL structure as shown in Fig. 3. The red-shift in infrared response from samples A to C consists with the PL–PLE spectra in Fig. 2. The increase of intensity associated with the $\Psi_o$-to-$\Psi_{2D}$ transition from samples A to C is attributed to the most deeply bound $\Psi_{2D}$ state for sample C. Moreover, while sample A exhibits similar spectral response at both bias polarities, samples B and C show the voltage-tunable dual band detection in the region of 6–11 μm. Such a result can be attributed to the notable structural asymmetry (along the growth direction) for samples B and C with thick InGaAs cap layers. For sample B, when the polarity changes from negative to positive voltages, the ground state electrons are pushed near the InGaAs cap layer. Better wavefunction overlap between the $\Psi_o$ and the $\Psi_{2D}$ states results in stronger $\Psi_o$-to-$\Psi_{2D}$ response compared with the originally dominant $\Psi_o$-to-$\Psi_n$ response. For the same reason, in sample C, the $\Psi_o$-to-$\Psi_{2D}$ response is further enhanced so it becomes the only peak in the spectrum at positive bias with improved wavefunction coupling.

In order to clarify that the 2D QW state of the CE-DWELL structure is dominated by the InGaAs layer above QDs instead of the InGaAs layer underneath QDs, three samples with different thicknesses (5 nm, 4 nm, and 3 nm) of InGaAs cap layer but fixed total thickness (7 nm) of InGaAs layers in the CE-DWELL were also prepared. The PLE spectra of these samples at 77 K are compared in Fig. 4, in which the 2D state signal is marked by the arrows. With the top InGaAs layer becoming thinner and thinner, the 2D state energy peak shifts to a higher energy sequentially although the bottom InGaAs layer is thicker instead. Fig. 4 clearly shows that the 2D state of the CE-DWELL structure indeed stems from the InGaAs cap layer but not the InGaAs layer below QDs.

To examine the observed bias-dependent infrared response in samples B and C more carefully, the absolute responsivity of the $\Psi_o$-to-$\Psi_{2D}$ transition was compared. For sample B at −1.2 V and 77 K, the responsivity of the $\Psi_o$-to-$\Psi_{2D}$ peak was obtained to be 63 mA/W. It increased to 77 mA/W with the bias voltage changed to +1.2 V. The enhancement of the $\Psi_o$-to-$\Psi_{2D}$ peak with the bias polarity change was confirmed to be not only relative to the $\Psi_o$-to-$\Psi_n$ peak but absolute in responsivity. In the case of sample C, in which the $\Psi_{2D}$ state has the strongest wavefunction confinement, the responsivity enhancement of the $\Psi_o$-to-$\Psi_{2D}$ transition due to improved wavefunction coupling at positive bias is even more pronounced. It increases for more than ten times at 77 K when the applied voltage is changed from −1.2 V (44 mA/W) to +1.2 V (469 mA/W). This confirmed the explanation mentioned previously for the complicated photocurrent spectra.

The influence of the thickness change of the InGaAs cap layer is not only on the optical property but also on the transport property of the devices. Noise measurement was executed to obtain the current gain of the devices. Assuming the generation–recombination noise dominates, the noise current gain of samples A–C is 104, 21, and 13 respectively at 77 K and −1.5 V. The thicker InGaAs cap layer increases the capture probability of the electrons moving across the well and the current gain is thus lowered [4]. The peak QE was then extracted from the responsivity and the current gain. Fig. 5 shows the peak QE of the three samples at different voltages and 77 K. Note that the peak QE refers to the $\Psi_o$-to-$\Psi_n$ transition for samples A and B but refers to the $\Psi_o$-to-$\Psi_{2D}$ transition for sample C. An asymmetric bias dependent behavior is clearly shown for all samples. For samples A and B, the peak QE of the $\Psi_o$-to-$\Psi_n$ transition is higher at negative bias because the ground state electron is pushed away from the InGaAs cap layer and the wavefunction coupling of the competing $\Psi_o$-to-$\Psi_{2D}$ transition is restrained. On the other hand, for sample C, the QE is higher at positive bias because the leading $\Psi_o$-to-$\Psi_{2D}$ transition peak is further enhanced with the ground state electron attracted to the InGaAs cap layer when biased positively. When the voltage applied for sample C is changed from −1.5 V to +1.5 V, the QE is dramatically increased from 0.2% to 2.4%. It is also noticed that sample A has higher peak QE than samples B and C because of the focused absorption strength. The highest QE measured for sample A reaches 7.23% (a respectable value for the 10-stacked QDIPs) at −1.05 V, demonstrating the power of the CE-DWELL structure. While for samples B and C with prominent dual band response, the carrier absorption is distributed over a wider spectral range and the peak QE suffers. For sample B, the highest QE is 1% at −1.2 V; but for sample C, the highest QE is 2.8% at 1.65 V. Finally, the highest detectivity

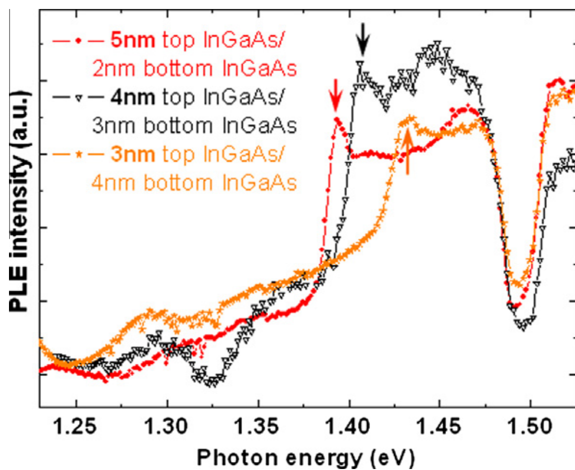


**Fig. 4.** 77 K PLE spectra of the CE-DWELL structures with different thicknesses of InGaAs cap layer but fixed total InGaAs thickness of 7 nm.

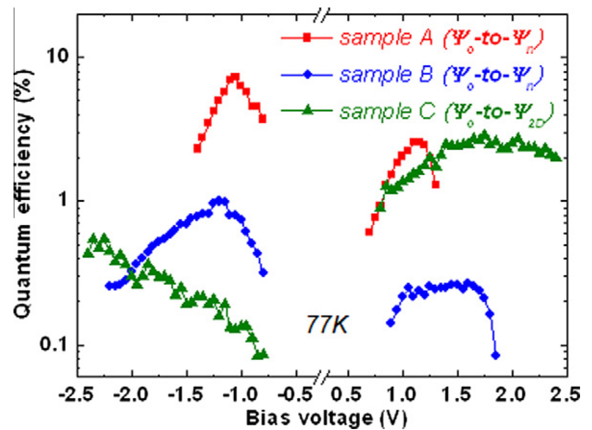


**Fig. 5.** The QE of the specific transition path at different voltages of each sample at 77 K.

measured for samples A–C at 77 K is $3.4 \times 10^{10}$ Jones, $4.5 \times 10^{9}$ Jones, and $5.8 \times 10^{9}$ Jones respectively.

## 4. Summary

In summary, we report the spectral response and device performance tuning for InAs QDIPs by selecting different intersubband transitions via adjusting the thickness of InGaAs cap layer in the CE-DWELL structure. Increasing the cap-layer thickness is found beneficial for the selection of the QD-to-QW transition path. The results in this study demonstrate the manipulation flexibility of the CE-DWELL QDIPs. For voltage-tunable multi-color detection, thick InGaAs cap layers are used; but for higher peak quantum efficiency, thin cap layers are preferred for the narrower absorption width of the transition between QD states. For the sample with 3 nm InGaAs cap layers, a respectable quantum efficiency of 7.23% is reached for 10-stack QDIPs with 7 μm detection wavelength at 77 K.

## Reference

[1] S. Chakrabarti, A.D. Stiff-Roberts, P. Bhattacharya, S. Gunapala, S. Bandara, S.B. Rafol, S.W. Kennerly, High-temperature operation of InAs–GaAs quantum-dot infrared photodetectors with large responsivity and detectivity, IEEE Photon. Technol. Lett. 16 (5) (2004) 1361–1363.

[2] P. Bhattacharya, X.H. Su, S. Chakrabarti, G. Ariyawansa, A.G.U. Perera, Characteristics of a tunneling quantum-dot infrared photodetector operating at room temperature, Appl. Phys. Lett. 86 (2005) 191106.

[3] H. Lim, S. Tsao, W. Zhang, M. Razeghia, High-performance InAs quantum-dot infrared photodetectors grown on InP substrate operating at room temperature, Appl. Phys. Lett. 90 (2007) 131112.

[4] S.Y. Wang, M.C. Lo, H.Y. Hsiao, H.S. Ling, C.P. Lee, Temperature dependent responsivity of quantum dot infrared photodetectors, Infrared. Phys. Technol. 50 (2007) 166–170.

[5] D.Z.Y. Ting, S.V. Bandara, S.D. Gunapala, J.M. Mumolo, S.A. Keo, C.J. Hill, J.K. Liu, E.R. Blazejewski, S.B. Rafol, Y.-C. Chang, Submonolayer quantum dot infrared photodetector, Appl. Phys. Lett. 94 (2009) 111107.

[6] S. Krishna, Quantum dots-in-a-well infrared photodetectors, Infrared. Phys. Technol. 47 (2005) 153–163.

[7] Y. Shah, J. Shao, T.E. Vandervelde, R.V. Shenoi, W.-Y. Jang, S. Krishna, Reduction in dark current using resonant tunneling barriers in quantum dots-in-a-well long wavelength infrared photodetector, Appl. Phys. Lett. 93 (2008) 131115.

[8] G. Jolley, L. Fu, H.H. Tan, C. Jagadish, J. Phys. D. 42 (2009) 095101.

[9] S.D. Gunapala, S.V. Bandara, C.J. Hill, D.Z. Ting, J.K. Liu, S.B. Rafol, E.R. Blazejewski, J.M. Mumolo, S.A. Keo, S. Krishna, Y.C. Chang, C.A. Shott, $640 \times 512$ pixels long-wavelength infrared (LWIR) quantum-dot infrared photodetector (QDIP) imaging focal plane array, IEEE J. Quantum Electron 43 (3) (2007) 230–237.

[10] H.S. Ling, S.Y. Wang, C.P. Lee, M.C. Lo, High quantum efficiency dots-in-a-well quantum dot infrared photodetectors with AlGaAs confinement enhancing layer, Appl. Phys. Lett. 92 (2008) 193506.

[11] H.S. Ling, S.Y. Wang, C.P. Lee, M.C. Lo, Long-wavelength quantum-dot infrared photodetectors with operating temperature over 200 K, IEEE Photon. Technol. Lett. 21 (2) (2009) 118–120.

[12] K. Muraki, S. Fukatsu, Y. Shiraki, R. Ito, Appl. Phys. Lett. 61 (1992) 557.

[13] L. Ouattara, A. Mikkelsen, E. Lundgren, et al., J. Appl. Phys. 100 (2006) 044320.